Journal of Solid State Chemistry **161,** 97–105 (2001)
doi:10.1006/jssc.2001.9289, available online at http://www.idealibrary.com on IDEAL®

Investigation of Mixed Divalent Cation Monophosphates: Synthesis, Crystal Structure, and Vibrational Study of $CdBa_2(HPO_4)_2(H_2PO_4)_2$

Lotfi Ben Taher,* Leila Smiri,*,[1] and Alain Bulou†

*Laboratoire de Chimie Inorganique et Structurale, Faculté des Sciences de Bizerte, 7021 Jarzouna, Tunisia; and
†Laboratoire de Physique de l'Etat Condensé, UMR CNRS No. 6087, Faculté des Sciences, Université du Maine, Avenue O. Messiaen, 72085 Le Mans Cedex 9, France

Received May 3, 2001; in revised form June 14, 2001; accepted June 25, 2001; published online August 22, 2001

Chemical preparation, single-crystal X-ray structure, and infrared and polarized Raman spectra of a new cadmium dibarium bis(monohydrogen monophosphate) bis(dihydrogen monophosphate) are presented. The atomic arrangement consists of anionic layers formed by HPO_4^{2-} and $H_2PO_4^-$ groups connected to each other through strong hydrogen bonds, resulting in a two-dimensional network. These sheets are held together by six oxygen-coordinated Cd^{2+} and nine oxygen-coordinated Ba^{2+} ions to build a three-dimensional framework. An assignment of lattice and internal vibrations in terms of symmetry species and approximate type of motion is given. A comparison with the vibrational fundamentals of the PO_4^{3-} ion in the isostructural $CaBa_2(HPO_4)_2(H_2PO_4)_2$ ($CaBa_2$) is also discussed. Band positions are found to be largely independent of the positive ion. Crystal data for $CdBa_2(HPO_4)_2(H_2PO_4)_2$ ($CdBa_2$): $M = 773.08\ g\ mol^{-1}$, monoclinic, space group $P2_1/c$ (No. 14), $a = 5.434(4)$ Å, $b = 10.140(2)$ Å, $c = 12.298(2)$ Å, $\beta = 100.43(3)^\circ$, $Z = 2$, $R_1/wR_2 = 0.024/0.066$ [1858 observed reflections with $I > 6\sigma(I)$]. © 2001 Academic Press

Key Words: **chemical preparation; cadmium; barium; phosphate; crystal structure; vibrational spectra.**

INTRODUCTION

Divalent cation phosphates with the general formula $M_n(H_mPO_4)_p$ are of interest for a number of reasons, one of which is that they can form a zeolite-like framework structure (1). We published the structure and some properties of a new strontium phosphate form, γ-$SrHPO_4$ (2). The system $M_3(PO_4)_2$–$M'_3(PO_4)_2$–xH_2O has also been extensively studied. For example, the nickel compounds $A_2Ni(PO_4)_2$, with A = Ba, Sr, were investigated because of their potential magnetic properties (3, 4). However, very little work was done on the hydrogen phosphate analogous system. In previous papers we have reported the preparation and the characterization (X-ray structure, IR spectroscopy, etc.) of the H-bonded crystals: $CaBa_2(HPO_4)_2(H_2PO_4)_2$ ($CaBa_2$) (5), $CdBa_2(HPO_4)(P_2O_7)$ (6), and $CaBa(HPO_4)_2$ (7). The latter, like γ-$SrHPO_4$ has H-bonded HPO_4^{2-} entities, where closed dimers are present along with infinite zigzag chains.

Several authors reported the vibrational properties of compounds containing HPO_4^{2-} groups. The monohydrogenmonophosphate ion, had different conformations (8–13) and peculiar bonding features depending on the environment and the nature of the cations. Vibrational spectra of the $H_2PO_4^-$ were also widely investigated. Again, for the reasons mentioned above, this ion is known to exist in different geometries (9, 14–16), for example, Hubert Joe *et al.* (16) assigned the FT-IR and polarized Raman spectra of $N(CH_3)_4H_2PO_4 \cdot H_2O$ on the basis of C_{2v} symmetry of the phosphate ion. It should be noticed that in spite of the simple structure of these anions, some disagreements were found in the literature, this is particularly important when interpreting the high-frequency H-modes region. To our knowledge, only one paper was published on compounds containing both HPO_4^{2-} and $H_2PO_4^-$: the IR and Raman spectra of $Te(OH)_6 \cdot 2NH_4H_2PO_4 \cdot (NH_4)_2HPO_4$ were reported by Viswanathan *et al.* (17). However, from their vibrational analysis the authors concluded that the hydrogen atoms are not strongly bonded to the oxygen atoms of phosphate groups and hence the phosphate ions exist as PO_4^{3-} ions rather than as HPO_4^{2-} and $H_2PO_4^-$ groups.

We therefore recorded the infrared and polarized Raman spectra of $CdBa_2$ and then we proposed a vibrational analysis in terms of the crystalline symmetry in order to confirm the structure and to contribute to the spectroscopic studies of the mixed monohydrogen–dihydrogen monophosphates. Comparison to the crystal structure and vibrational data of some related compound were also given.

[1] To whom correspondence should be addressed. E-mail: leila.smiri@fsb.rnu.tn. Fax: 216 2 590 566.

0022-4596/01 $35.00

EXPERIMENTAL

Crystals of $CdBa_2$ were prepared by the hydrothermal method as follows:

$$CdCO_3 + 2BaCO_3 + 4H_3PO_4 \rightarrow CdBa_2(HPO_4)_2(H_2PO_4)_2 + 3CO_2 + 3H_2O.$$

The mixture of starting materials ($Cd:Ba:P:H_2O = 1:2:22:650$) was placed in a Teflon-coated steel autoclave, which was approximately 80% full. The bomb was heated at 140°C under autogeneous pressure for 1 day and then cooled to room temperature. Numerous transparent needle-shaped crystals were filtered off, washed with distilled water and air dried overnight at 50°C.

TABLE 1
Summary of Crystal Data, Intensity Measurements, and Refinement Parameters for $CdBa_2(HPO_4)_2(H_2PO_4)_2$

Crystal data	
Formula	$CdBa_2(HPO_4)_2(H_2PO_4)_2$
Formula weight ($g\,mol^{-1}$)	773.08
Crystal dimensions (mm^3)	$0.36 \times 0.19 \times 0.15$
Habit, color	Needle, colorless
Crystal system	Monoclinic
Space group	$P2_1/c$ (No. 14)
Cell dimensions (Å, °)	$a = 5.434(4)$, $b = 10.140(2)$, $\beta = 100.43(3)$, $c = 12.298(2)$
V (Å^3), Z	664.6(6), 2
ρ_{calcd} ($g\,cm^{-3}$)	3.850
Absorption coefficient (mm^{-1})	μ (Mo$K\alpha$) = 7.99
Intensity measurements	
Temperature (K)	293(2)
Radiation, λ (Å)	Mo$K\alpha$, 0.71073
Scan mode (°)	ω
Scan width (°)	1.2
2θ range (°)	3.37–29.97
hkl limits	$-7 \le h \le 7$, $-3 \le k \le 14$, $-5 \le l \le 17$
Independent reflections	1939 ($R_{int} = 0.217$)
Observed reflections [$I > 6\sigma(I)$]	1858
Min/Max transmission	0.3060/0.7438
Structure solution and refinement	
Structure solution	Patterson
Structure refinement	Full-matrix against on F^2
Parameters refined	119
Goodness of fit	$S = 1.226$
Reliability factors[a] [$I > 6\sigma(I)$]	$R_1 = 0.024$ (0.0254 for all data), $wR_2 = 0.066$
Extinction coefficient	0.024
$\Delta\rho_{min/max}$ ($e\,Å^{-3}$)	−1.07/1.62

[a] R values are defined as $R_1 = \sum \| F_o| - |F_c \| / \sum |F_o|$ and $wR_2 = [\sum w(F_o^2 - F_c^2)^2 / \sum w(F_o^2)^2]^{1/2}$, where $w^{-1} = [\sigma^2(F_o^2) + (0.0346P)^2 + 2.36P]$ and $P = (F_o^2 + 2F_o^2)/3$.

TABLE 2
Atomic Coordinates and Equivalent Isotropic Displacement Parameters (Å × 10^4) for $CdBa_2(HPO_4)_2(H_2PO_4)_2$

Atom	x	y	z	U_{eq}[a]
Ba(1)	0.13913(4)	0.84601(2)	0.3234(2)	145(1)
Cd(1)	0	0	0	114(1)
P(1)	−0.2346(2)	0.80331(9)	0.55301(7)	110(2)
P(2)	0.4147(2)	0.51083(9)	0.30196(7)	105(2)
O(1)	−0.2380(5)	0.9516(3)	0.5167(2)	165(5)
O(2)	−0.5166(5)	0.7616(3)	0.5193(2)	168(5)
O(3)	−0.1583(5)	0.8030(3)	0.6767(2)	178(5)
O(4)	−0.0709(5)	0.7244(3)	0.4901(2)	174(5)
O(5)	0.4785(6)	0.6608(3)	0.2851(2)	158(12)
O(6)	0.6374(5)	0.4451(3)	0.3756(2)	171(5)
O(7)	0.3735(5)	0.4432(3)	0.1899(2)	169(5)
O(8)	0.1772(5)	0.5137(3)	0.3496(2)	187(5)
H(1)	−0.28(1)	0.976(7)	0.457(5)	330(170)[b]
H(2)	−0.57(1)	0.695(6)	0.545(5)	220(140)[b]
H(5)	0.60(1)	0.669(8)	0.261(7)	600(200)[b]

[a] $U_{eq} = \frac{1}{3}\sum_i \sum_j U_{ij} a_i^* a_j^* a_i a_j$.
[b] U_{iso}.

It is interesting to note that for the composition ($Cd:Ba:P:H_2O = 1:2:6:178$) and at room temperature, we have initially obtained pure microcrystalline powder for this phase. Preliminary X-ray powder data (Philips PW 3710, $\lambda = 1.5418$ Å, flat-plate sample, θ–2θ scan mode) could be indexed using the program Treor (18), $CdBa_2$ was found to be isostructural with $CaBa_2$. A least-squares refinement (U-FIT (19)) of the resulting powder pattern leads to the unit-cell dimensions: $a = 5.433(2)$ Å, $b = 10.134(2)$ Å, $c = 12.272(3)$ Å, and $\beta = 100.39(3)°$.

Single-crystal X-ray intensity data were obtained at room temperature from an as-synthesized specimen measuring $0.36 \times 0.19 \times 0.15\,mm^3$. Data were collected on an Enraf-Nonius CAD4 four-circle diffractometer. The unit cell parameters were determined by a least-squares fit of randomly located reflections between 20° and 24° in 2θ. Data reduction, absorption correction (option SHELXA), initial heavy-atom positions (Cd, Ba, P), and refinements were carried out with the use of programs in the WinGX package (20). A final difference synthesis clearly revealed the hydrogen-atom coordinates, and bond distances constraints [$d_{O-H} = 0.9 \pm 0.05$ Å] were applied to stabilize the least-squares refinement of the H positions. Crystallographic data and some details of the structure refinement are summarized in Table 1. The existence of an O–H···O bridges between O(1) and O(7), O(2) and O(6), and O(5) and O(3) is suggested by their anomalously low bond valence sums (BVS) (21), compared to the expected value of 2 (Table 4).

IR data were collected in the range 370–4000 cm^{-1} with a Perkin-Elmer FT-IR Spectrum 1000 PC spectrophotometer using the KBr pellet technique. Spectral resolution was better than 4 cm^{-1}.

TABLE 3
Selected Interatomic Distances (Å) and Angles (°) for $CdBa_2(HPO_4)_2(H_2PO_4)_2$

$Ba(1)O_9$ polyhedron $\langle Ba–O \rangle = 2.868(3)$ Å			
Ba(1)–O(1)$^{(iv)}$	2.825(3)	Ba(1)–O(6)$^{(vii)}$	3.091(3)
Ba(1)–O(2)$^{(v)}$	2.899(3)	Ba(1)–O(7)$^{(vii)}$	2.859(3)
Ba(1)–O(3)$^{(vi)}$	2.663(3)	Ba(1)–O(7)$^{(i)}$	2.932(3)
Ba(1)–O(4)	2.806(3)	Ba(1)–O(8)$^{(i)}$	3.008(3)
Ba(1)–O(5)	2.732(3)		

$Cd(1)O_6$ octahedron $\langle Cd–O \rangle = 2.293(3)$ Å						
Cd(1)	O(4)$^{(viii)}$	O(4)$^{(ix)}$	O(6)$^{(x)}$	O(6)$^{(xi)}$	O(8)$^{(viii)}$	O(8)$^{(ix)}$
O(4)$^{(viii)}$	**2.307(3)**	4.614(5)	3.422(4)	3.134(4)	3.196(4)	3.234(4)
O(4)$^{(ix)}$	180	**2.307(3)**	3.134(4)	3.422(4)	3.234(4)	3.196(4)
O(6)$^{(x)}$	95.0(1)	85.0(1)	**2.333(3)**	4.666(5)	3.088(4)	3.373(4)
O(6)$^{(xi)}$	85.0(1)	95.0(1)	180	**2.333(3)**	3.373(4)	3.088(4)
O(8)$^{(viii)}$	89.3(1)	90.7(1)	84.9(1)	95.1(1)	**2.239(3)**	4.478(5)
O(8)$^{(ix)}$	90.7(1)	89.3(1)	95.1(1)	84.9(1)	180	**2.239(3)**

$P(1)O_4$ tetrahedron $\langle P–O \rangle = 1.537(6)$ Å				
P(1)	O(1)	O(2)	O(3)	O(4)
O(1)	**1.567(3)**	2.454(4)	2.454(4)	2.519(4)
O(2)	102.9(2)	**1.572(3)**	2.520(4)	2.541(4)
O(3)	106.1(2)	110.1(2)	**1.503(3)**	2.553(4)
O(4)	109.9(2)	111.1(2)	115.9(2)	**1.509(3)**
P(1)–O(1)–H(1)		124(5)°		
P(1)–O(2)–H(2)		123(4)°		

$P(2)O_4$ tetrahedron $\langle P–O \rangle = 1.539(6)$ Å				
P(2)	O(5)	O(6)	O(7)	O(8)
O(5)	**1.582(3)**	2.53(4)	2.515(4)	2.451(4)
O(6)	109.2(2)	**1.527(3)**	2.467(4)	2560(4)
O(7)	108.4(2)	108.2(2)	**1.519(3)**	2.503(4)
O(8)	104.8(2)	114.8(2)	111.3(2)	**1.512(3)**
P(2)–O(5)–H(5)		11(6)°		

Hydrogen bonding scheme

D–H···A	D–H (Å)	H···A (Å)	D···A (Å)	D–H···A (°)
O(1)–H(1)···O(7)$^{(i)}$	0.76(6)	1.81(6)	2.515(4)	150(7)
O(2)–H(2)···O(6)$^{(ii)}$	0.84(5)	1.78(6)	2.608(4)	166(6)
O(5)–H(5)···O(3)$^{(iii)}$	0.81(7)	1.80(7)	2.600(4)	166(9)

Note. Symmetry codes: (i) $-x, y+\frac{1}{2}, -z+\frac{1}{2}$; (ii) $-x, -y+1, -z+1$; (iii) $x+1, -y+\frac{3}{2}, z-\frac{1}{2}$; (iv) $-x, -y+2, -z+1$; (v) $x+1, y+2, z$; (vi) $x, -y+\frac{3}{2}, z-\frac{1}{2}$; (vii) $-x+1, y+\frac{1}{2}, -z+\frac{1}{2}$; (viii) $x, -y+\frac{1}{2}, z-\frac{1}{2}$; (ix) $-x, y-\frac{1}{2}, -z+\frac{1}{2}$; (x) $x-1, -y+\frac{1}{2}, z-\frac{1}{2}$; (xi) $-x+1, y-\frac{1}{2}, -z+\frac{1}{2}$.

Cell parameters were checked and crystal faces indexed on a four-circle diffractometer (AED2 Siemens-Stoe, $\lambda = 0.71069$ Å, 293(2) K) for single crystals used for Raman experiments.

Raman spectra were obtained on a Dilor Z24 triple monochromator with multichannel (CCD) detection and 514.5 nm Ar^+ ion laser (Coherent Innova 90.3) excitation source with 100 mW power. All measurements were conducted at room temperature under an $\times 50$ objective microscope in a backscattering geometry. This was performed on micrometric samples (typically less than 1 mm in length) fixed on a goniometer head and suitably oriented for polarization analysis. The polarized spectra were recorded under various polarization configurations (polarizer + analyzer).

TABLE 4
Bond Valence Analysis of $CdBa_2(HPO_4)_2(H_2PO_4)_2$[a]

	O(1)[b]	O(2)[b]	O(3)	O(4)	O(5)[b]	O(6)	O(7)	O(8)	Σ_s
Ba(1)	0.23	0.19	0.36	0.24	0.30	0.11	0.21 + 0.17	0.14	1.95
Cd(1)				2×0.34		2×0.31		2×0.40	2.10
P(1)	1.10	1.09	1.31	1.29					4.79
P(2)					1.06	1.23	1.26	1.28	4.83
Σ_s	1.33	1.28	1.67	2.21	1.36	1.96	1.64	2.22	

[a] The results refer to the equation $s = \exp[(r_0 - r)/0.37]$ with $r_0 = 2.285$, 1.904, and 1.604 for Ba^{2+}–O, Cd^{2+}–O, and P^{5+}–O, respectively.
[b] O–H groups.

The instrumental resolution was better than 1 cm^{-1}. In order to gain intensity, the high-frequency H-modes range (1500–3500 cm^{-1}) was investigated with a single monochromator and without polarization. Moreover, to elucidate the main characteristics of the spectra, its is useful to do a comparison with the isomorphic $CaBa_2$. So we have performed the IR spectrum and the unpolarized (we have been unable to prepare correctly oriented crystals) Raman data in the low-frequency region of this compound under the same experimental conditions of $CdBa_2$.

RESULTS AND DISCUSSION

A. Structure

Atomic positional and equivalent isotropic thermal parameters are listed in Table 2, with selected bond distance/angle data presented in Table 3. As shown from the projection of the structure onto (001) plane (Fig. 1), the structural arrangement consists of a succession along [100] of anionic layers of $H_2P(1)O_4^-/HP(2)O_4^{2-}$ groups (hereafter referred as P1/P2). Adjacent sheets are bound to each other through Ba^{2+} and Cd^{2+} cations, resulting in a three-dimentional network. Intrasheet hydrogen bonds offer additional stability to the structure.

Ba^{2+} is 9-coordinated to oxygen atoms within ~ 3 Å. This choice is in agreement with results of BVS calculation. Adjacent BaO_9 polyhedra are linked via O(7) into infinite ribbons, similar to the situations found in $CaBa_2$ and $CaBa(HPO_4)_2$.

The Cd ion located on an inversion center has a rather regular octahedral coordination, with Cd–O distances ranging from 2.239 to 2.333 Å. and O–Cd–O angles from 84.9 to 95.1°. It must be noticed that the little decrease of $CdBa_2$ cell parameters compared with those of $CaBa_2$ ($a = 5.4902(7)$ Å, $b = 10.2004(12)$ Å, $c = 12.373(3)$ Å, $\beta = 100.783(14)°$, $V = 680.7(2)$ Å^3) is caused by a cations radius change, where Ca^{2+} ions, ($r_{VI}(Ca^{2+}) = 1.00$ Å) are replaced by the slightly smaller Cd^{2+} ($r_{VI}(Cd^{2+}) = 0.95$ Å) ones (22).

The two P1/P2 hydrogen phosphate groups display typical tetrahedral geometry with $d_{av}(P(1)–O) = 1.537$ Å and

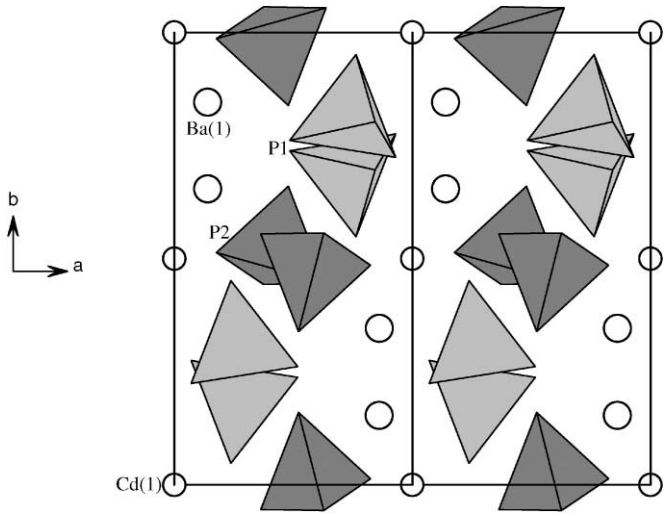

FIG. 1. [001] View of the $CdBa_2(HPO_4)_2(H_2PO_4)_2$ structure.

d_{av}(P(2)–O) = 1.539 Å. The longest distances, P(1)–O(1), P(1)–O(2), and P(2)–O(5), correspond to the P–O(H) bonds. Both P1 and P2 units are involved in strong hydrogen bonds (23) (Table 3). The overall hydrogen bonding scheme in $CdBa_2$ is illustrated in Fig. 2. There is a distribution of three donor (O–H) and three acceptor (O···H) functions between P1($2D + A$) and P2 ($D + 2A$). Here, we find the same connectivity as observed in the phosphate $CaBa_2$ and the sulfate $K(HSO_4)(H_2SO_4)$ (24); a P1 unit is linked by two strong hydrogen bonds (O(1)···O(7), 2.515 Å, O(3)···O(5), 2.600 Å) to the two adjacent P2 units and vice versa, resulting in hydrogen-bonded tetramers (2P1 + 2P2). Each of these tetramers is located on an inversion center, thus comprising two independent tetrahedra. One tetramer is connected to its four neighbors by four hydrogen bonds (O(2)···O(6): 2.608 Å), giving rise to an infinite two-dimensional hydrogen-bonded network lying parallel to the (100) plane. Besides, there is no H-bond connection between two adjacent nets.

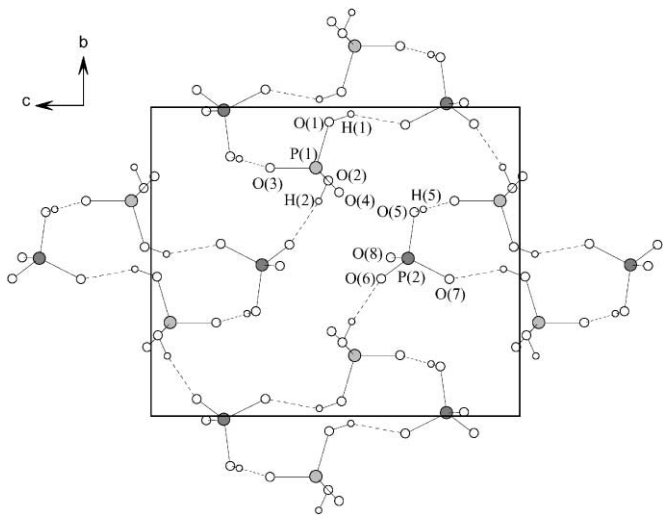

FIG. 2. The hydrogen bonding system in $CdBa_2(HPO_4)_2(H_2PO4)_2$.

B. Vibrational Spectra Analysis

Factor group analysis. $CdBa_2$ is monoclinic ($P2_1/c$, $Z = 2$) with Ba^{2+}, HPO_4^{2-}, and $H_2PO_4^-$ occupying C_1 sites, whereas Cd^{2+} atoms are placed in C_i sites. The factor group analysis (Table 5) using the standard correlation method (25) has been carried out to number the vibrations and determine the IR- and Raman-active modes. Excluding the acoustic modes, 171 normal modes are predicted. These are distributed as follows:

$$\Gamma = 42A_g + 42B_g + 44A_u + 43B_u,$$

where the g and the u modes are Raman- and IR-active, respectively. We should also note that except the Cd^{2+} translational modes which are forbidden in Raman, all vibrations are expected to appear in all factor group species.

Interpretation of the vibrational spectra. The vibrational spectra are shown in Figs. 3–6. The Raman spectra that we obtained consist of a number of distinct and well separated groups of bands and can be subdivided into four frequency regions: The low-frequency (50–350 cm^{-1}) region of lattice modes, the 380–600 and 800–1200 cm^{-1} regions of PO_4^{3-} internal bending and stretching modes, respectively, and the high-frequency (1200–3500 cm^{-1}) region of hydrogen motions. The IR spectra of $CdBa_2$ and $CaBa_2$ (Fig. 5), which appear very close to each other can be mainly subdivided into the three ranges: 370–600, 900–1200, and 1200–3500 cm^{-1}. Spectral data, relative intensities, and proposed vibrational assignments are listed in Table 6.

Internal modes of the PO_4^{3-} ions. The unperturbed PO_4^{3-} ion is a tetrahedron with point group symmetry T_d. The normal modes of vibrations have frequencies at approximately 938, 420, 1017, and 567 cm^{-1} for $v_1(A_1)$, $v_2(E)$, $v_3(F_2)$, and $v_4(F_2)$, respectively (26). All of these modes are Raman-active, whereas the triply degenerate v_3 and v_4 are IR. In the crystal, the symmetry of PO_4^{3-} ions is reduced from T_d to C_1, and therefore anisotopic crystal fields may lift degeneracies and allow inactive modes to be active (Table 5). Moreover, since some P–O distances in P1 and P2 are very close, there is a possibility for accidental degeneracy between the bands of these two groups. The interpretation of the spectra (particularly the lattice modes region) is complicated due to the presence of different types of ions in the unit cell.

From group theoretical predictions, four lines ($2A_g + 2B_g$) are expected in all orientations for the symmetric stretching mode v_1. The polarized Raman bands observed around 892 and 915 cm^{-1} are easily assigned to this mode.

TABLE 5
Vibrational Analysis of $CdBa_2(HPO_4)_2(H_2PO_4)_2$

Factor group C_{2h} $C_2 = y$	N	A	External modes				Internal modes: PO_4[a]				Internal modes: O–H ··· O			Activity	
			$T_{P1/P2}$	$R_{P1/P2}$	$T_{Cd^{2+}}$	$T_{Ba^{2+}}$	ν_1	ν_2	ν_3	ν_4	ν	β	γ	IR	Raman
A_g	42	0	6	6	0	3	1	2	3	3	3	3	3	—	(α_{xx}, α_{yy}, α_{zz}, α_{xz})
B_g	42	0	6	6	0	3	1	2	3	3	3	3	3	—	(α_{xy}, α_{zy})
A_u	45	−1	6	6	3	3	1	2	3	3	3	3	3	z	—
B_u	45	−2	6	6	3	3	1	2	3	3	3	3	3	(x, y)	—

Note. N, number of degrees of freedom: A, number of acoustic modes; T, number of translational modes; R, number of rotational modes.
[a] Symmetry of normal modes for each set of the two equivalent PO_4 (P1/P2) sites.

The additional broad line located around 938 cm^{-1} in xy (shoulder) and yy (weak band) orientations probably originates from the interaction between vibrating ions or may be ascribed to a γ_{O-H}, as pointed out by Marchon *et al.* (27) (the γ_{O-H} bands are usually very weak in Raman and thus overlapped by stronger ν_{P-O}). In IR their counterparts ($2A_u + 2B_u$) appear at 850, 892, 911, and 942 cm^{-1}. For $CaBa_2$, however, two bands are slightly shifted to lower wavenumbers (850, 886, 907, and 942 cm^{-1}), which could be related to the cation mass effect (Cd^{2+} is replaced by Ca^{2+}). We also note that bands in this range of frequencies are relatively strong, indicating the presence of either HPO_4^{2-} or $H_2PO_4^-$ ion (28).

For the asymmetric stretching mode ν_3, 12 Raman components ($6A_g + 6B_g$) are predicted in all polarization geometries. Only 10 bands ($5A_g + 5B_g$), however, have been observed between 984 and 1146 cm^{-1}, the totally symmetric A_g mode being much stronger than the B_g one. This is probably due to either accidental degeneracy or to overlapping by some broader bands such as this situated at 984 cm^{-1}. The large number of PO_4^{3-} ions with different P–O lengths in the unit cell gives rise to such a large splitting (162 cm^{-1}). In IR, the group of bands in the 990–1160 cm^{-1} region is assigned to this mode. These bands are relatively broad and their number is smaller than predicted, which could be due to overlapping. It is to be noted that in the case of $CaBa_2$, bands due to this mode are also slightly shifted, but toward higher wavenumbers.

The symmetric bending mode ν_2 is found in the 385–415 cm^{-1} region with degeneracy totally lifted in Raman, whereas only three bands are observed in the IR spectra.

The asymmetric bending mode ν_4 (502–571 cm^{-1}) also appear with degeneracy completely removed; Raman spectra clearly show six lines for each symmetry specie as

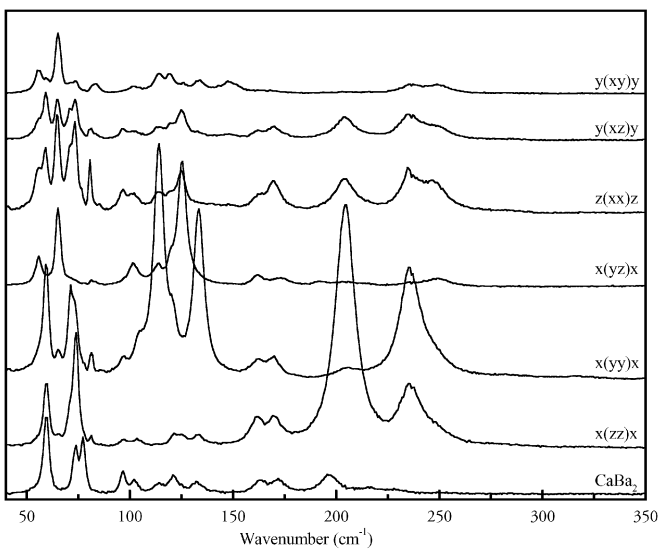

FIG. 3. Polarized Raman spectra (with comparison to $CaBa_2(HPO_4)_2(H_2PO_4)_2$) of $CdBa_2(HPO_4)_2(H_2PO_4)_2$ (10–350 cm^{-1}).

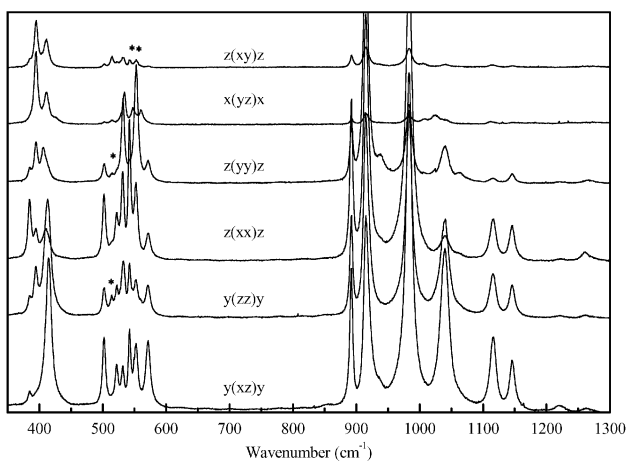

FIG. 4. Polarized Raman spectra of $CdBa_2(HPO_4)_2(H_2PO_4)_2$ (350–1300 cm^{-1}) (* arose from polarization leakage).

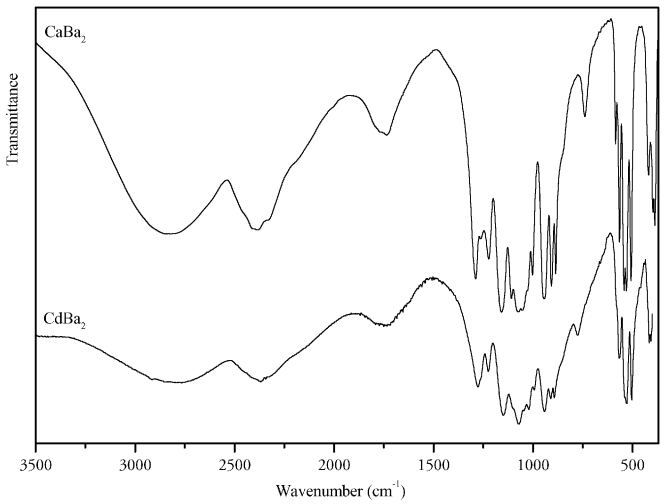

FIG. 5. Infrared spectra of $CdBa_2(HPO_4)_2(H_2PO_4)_2$ and $CaBa_2(HPO_4)_2(H_2PO_4)_2$.

can be expected from the lowering of the symmetry of ions from T_d to C_1, whereas it is partially retained in IR. Again, as mentioned above for the symmetric and asymmetric stretching modes, the corresponding bending modes are also shifted in the same manner (reversed) in the spectra of the two isostructural phases, but ν_2 is found to be slightly more sensitive to cation substitution.

In summary, it seems interesting to note the following for the internal modes of the PO_4^{3-} ion:

(i) Degeneracies are almost totally lifted (Davidov splitting), supporting strong correlation field in the crystals.

(ii) The influence of the cations on the vibrational fundamentals do not appear very marked and no systematic correlation between frequency and increasing mass of the positive ion could be found. Thus, these shifts are probably bounded up with the tendency for formation of cation–oxygen covalent bonds. Strong hydrogen bonds established between phosphate ions may also be significant.

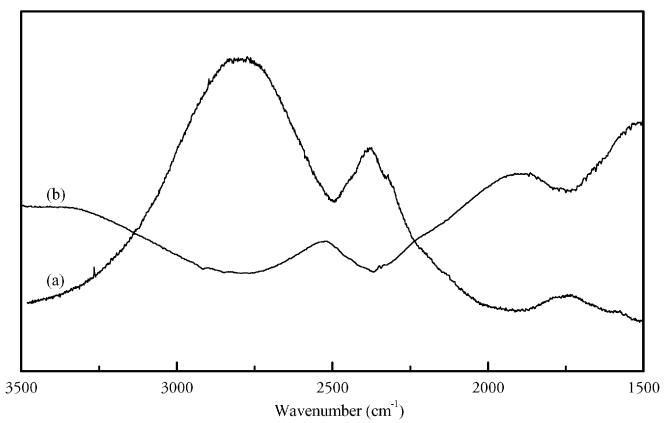

FIG. 6. Raman (a) and infrared (b) spectra of $CdBa_2(HPO_4)_2(H_2PO_4)_2$ (1500–3500 cm^{-1}).

O–H groups vibrations. The ABC-type broad bands of high-frequency H-vibrations have been interpreted as O–H stretching modes in Fermi resonance with combination involving mainly O–H bending vibrations (29) or in terms of strong coupling between fast O–H and slow O···O stretching modes (30). These spectral characteristics have been observed in a variety of strong hydrogen bonded solids having O···O distances varying from 2.45 to 2.66 Å, $CaBa(HPO_4)_2$ (7), $N(CH_3)_4H_2PO_4 \cdot H_2O$ (16), and NaH_2PO_4 (31) being examples. In the present case, these bands (Fig. 6) appear in the regions 2500–3400, 2000–2500, and 1520–1877 cm^{-1}, respectively. According to the correlation curve $\nu_{O\text{–}Hi}$ vs(Ri = O–Hi···O) established by Choi *et al.* (31) for some hydrogen monophosphates, -sulfates, and -arseniates, the extremely broad and intense A-type band could be interpreted as an overlapping of three bands of A-type whose maxima corresponding to each of the three O–H···O bonds: $\nu_{O\text{–}H1}(R1 = 2.515\,Å) = 2687\ cm^{-1}$, $\nu_{O\text{–}H2}(R2 = 2.600\,Å) = 2827\ cm^{-1}$, and $\nu_{O\text{–}H5}(R5 = 2.608\,Å) = 2840\ cm^{-1}$. While this band is more pronounced in the IR spectrum of $CaBa_2$, and the maximum is shifted to higher frequencies at about 86 cm^{-1}. The result is well known: A-type band frequency increases with increase in bond length ($CaBa_2$: $R1 = 2.507$ Å, $R2 = 2.613$ Å, $R5 = 2.666$ Å) and the intensities of B and C bands are often transferred to the A band (30). The contour of the B band shows two maxima lying at 2368 and 2306 cm^{-1} and a shoulder situated around 2140 cm^{-1}, these bands may be correlated with the presence of the three different H-bond lengths $R1$, $R2$, and $R5$. Band C ($\sim$1749 cm^{-1}) could be a combination of the P–O and P–O(H) stretching vibrations.

As in other phosphates (9, 27), the $\beta_{O\text{–}H}$ in-plane-bending vibrations occur in the region 1200–1400 cm^{-1}. As expected, the triplet observed in both Raman and IR spectra in the range 1220–1290 cm^{-1} is attributed to this mode. These wavenumbers are associated with the three different kinds of O–H···O bonds present in the crystal structure; the high-frequency band being assigned to the short hydrogen bond, whereas the low-frequency band is assigned to the long hydrogen bond.

The $\gamma_{O\text{–}H}$ out-of-plane-bending vibrations, on the other hand, are characterized by a single band in IR spectra (775 cm^{-1} for $CdBa_2$ and 739 cm^{-1} for $CaBa_2$), while as outlined above, it could be the line exhibiting at 938 cm^{-1} in Raman.

External modes. All the Raman bands (Fig. 3) observed in the region below 300 cm^{-1} must be due to lattice vibrations, since the lowest internal mode frequency is found at 385 cm^{-1}. On the other hand, the unit cell contains a large

TABLE 6
Assignments[a] of the Observed Spectra of $CdBa_2(HPO_4)_2(H_2PO_4)_2$ with IR and Low-Frequency Raman Data Comparison with $CaBa_2(HPO_4)_2(H_2PO_4)_2$

Raman (cm^{-1})							IR (cm^{-1})		
α_{xx}	α_{yy}	α_{zz}	α_{xz}	α_{xy}	α_{yz}	$CaBa_2$	$CdBa_2$	$CaBa_2$	Assignments
56 w			56 w	56 m	56 m				External modes
59 w	59 m	59 m	59 s	60 w		60 s			
65 m	66 vw	65 vw	65 s	66 vs	66 s				
72 sh	71 m	71 sh	71 m						
74 m	74 sh	74 m	74 m	74 w		74 m			
82 w	82 w	82 vw	82 w	83 m	82 w	77 m			
97 vw	97 vw	97 vw	97 w			97 w			
				102 w	102 m	102 w			
104 vw	105 vw	105 vw	104 w						
114 vw	114 s	114 vw	114 w	115 m	114 m	114 w			
	120 w		120 w	120 m	120 sh	121 w			
125 w		125 vw	125 m		125 vs				
	135 s	134 vw		134 w		132 w			
				148 m					
162 vw	162 w	162 w	162 m		162 w	163 w			
170 w	170 w	170 w	170 m			172 w			
					174 w				
205 w	205 vw	205 s	205 w		205 w	197 w			
237 w	236 m	236 m	236 w	237 m, br		217 vw			
248 w			248 w			219 vw			
				251 m, br	251 w				
385 m	385 w	386 w	385 vw	385 vw			407 m	388 m	$\nu_2(\delta_{O\text{-}P\text{-}O})$
395 w	395 m	395 m		395 vs	395 vs				
406 w	406 m						416 m	398 m	
				411 s	411 s		423 sh	419 m	
		414 s	415 s						
502 m	502 w	502 w	502 m						$\nu_4(\delta_{O\text{-}P\text{-}O})$
				504 vw	504 vw		504 s	507 s	
	*515 vw	*515 vw		515 vw	515 vw				
522 w		522 w	522 w				528 s	530 s	
531 m	532 s	532 m	532 w	532 vw			539 s	542 s	
					534 s				
542 s		542 m	542 m	*542 vw					
					548 m				
553 m	553 s	553 w	553 m	*553 vw					
					561 m		565 m	565 w	
571 w	571 w	571 w	571 m				581 sh	584 m	
							775 w	739 m	$\gamma_{O\text{-}H}$
							850 sh	850 sh	$\nu_1(\nu_{P\text{-}O})$
892 s	892 m	892 s	892 s	892 m	892 w		892 s	886 s	
915 s	914 vs	914 vs	914 s	914 m	914 m		911 s	907 s	
	938 w		938 sh				942 s	942 s	
984 vs	984 s	984 vs	984 vs	984 m	984 m		994 w	1002 m	$\nu_3(\nu_{P\text{-}O})$
					1004 w		1019 s	1025 s	
					1009 w		1044 vw	1051 s	
					1025 w		1073 vs	1076 s	
1040 w	1040 m	1040 s	1040 s	1040 vw	1040 vw		1102 sh	1109 m	
1063 vw	1063 w						1151 s	1160 s	
				1114 vw	1113 vw				
1116 w	1116 w	1116 m	1116 m						
1146 w	1146 w	1146 m	1146 m	*1146 vw, br	*1146 vw				

TABLE 6—*Continued*

Raman (cm^{-1})							IR (cm^{-1})		
α_{xx}	α_{yy}	α_{zz}	α_{xz}	α_{xy}	α_{yz}	$CaBa_2$	$CdBa_2$	$CaBa_2$	Assignments
1221 vw, br	1221 vw, br	1221 vw, br	1221 w, br				1226 m	1223 m	β_{O-H}
1263 w, br		1263 vw, br	1263 w, br				1264 sh	1261 vw	
	1267 vw, br						1279 s	1289 s	
**1742 br							1749 m, br	1730 m, br	Combination (band C)
**2210 sh							2199 sh	2189 sh	ν_{O-H} (band B)
**2332 sh							2315 s	2333 s	
**2389 m, br							2370 s	2394 s	
							2460 sh		
**2807 s, br							2750 s, br	2836 s, br	ν_{O-H} (band A)

[a] Relative intensities: s, strong; vs, very strong; m, medium; w, weak; vw, very weak; shoulder; br, broad; ν, stretching; δ, bending; β, in-plane bending; γ, out-of-plane bending.

* Arose from polarization leakage.

** Recorded with a single monchromator and without polarization (see text).

number of the same type of ions, the phonon energies will be closely spaced, and hence all predicted modes could not be observed. In addition to the lattice vibrations described by the group theoretical analysis, it is possible to observe the low-frequency stretching vibrations of the hydrogen-bonded oxygen atoms (O···O). According to previous articles (32, 33), the translational modes associated with Ba^{2+} are found below 150 cm^{-1}. Therefore, in our spectra these vibrations should appear among the group of bands in the region 56–140 cm^{-1}. Furthermore, since Ba^{2+} have the same environment in $CdBa_2$ and $CaBa_2$ (BaO_9 polyhedra with d_{av}Ba–O = 2.868 and 2.880 Å in $CdBa_2$ and $CaBa_2$, respectively), the corresponding vibrational lines should appear at the same position for both crystals. These lines (taking account for instrumental resolution) are 60, 74, 97, 102, 114, and 120 cm^{-1}. Finally, the assignment of the remaining bands over the low-frequency region is very complicated; since there are different P1/P2 groups with different O–H···O bridges, the $\delta_{O\cdots O}$, $\nu_{O\cdots O}$, $T_{P1/P2}$, and $R_{P1/P2}$ are believed to be regularly spread (27).

CONCLUSION

The crystal structure of $CdBa_2(HPO_4)_2(H_2PO_4)_2$ has been determined from single-crystal X-ray diffraction data. The relationships with other related structures have also been discussed.

The infrared and Raman spectra of the title compound have been measured and studied in detail on the basis of group theoretical analysis and by reference to other related compounds. The vibrational spectra confirm the structural features obtained from of the X-ray data. In particular:

(a) The observation of the inactive ν_1 and ν_2 in the infrared spectra and the lifting of degeneracies of ν_2, ν_3, and ν_4 modes suggest that the PO_4 tetrahedron is distorted confirming the X-ray study.

(b) The large splitting for the ν_3 mode indicates the presence of different phosphate ions in the crystal structure.

(c) ABC bands are observed in the O–H stretching region in both infrared and Raman spectra confirming the presence of strong hydrogen-bonded systems.

(d) From infrared data comparison with the isostructural compound $CaBa_2(HPO_4)_2(H_2PO_4)_2$, we have deduced that the frequencies corresponding to the fundamentals of the PO_4^{3-} are slightly sensitive to cation replacement. In addition, we have successfully identified the $T_{Ba^{2+}}$ frequencies.

ACKNOWLEDGMENTS

The authors express their sincere thanks to Professor M. Leblanc (Laboratoire des Fluorures, UPRES-A CNRS 6010, Faculté des Sciences, Université du Maine, Le Mans, France) for his collaboration.

REFERENCES

1. T. E. Gier and G. D. Stucky, *Nature* **349,** 508 (1991).
2. L. B. Taher, L. Smiri, Y. Laligant, and V. Maisonneuve, *J. Solid State Chem.* **152,** 428 (2000).
3. B. Elbali, A. Boukhari, J. Aride, M. Belaiche, F. Abraham, and M. Drillon, *Eur. J. Solid State Inorg. Chem.* **31,** 61 (1994).
4. B. Elbali, A. Boukhari, E. M. Holt, and J. Aride, *Acta Crystallogr. C* **49,** 1131 (1993).
5. L. B. Taher, L. Smiri, and A. Driss, *Acta Crystallogr. C* **55,** 1757 (1999).
6. L. B. Taher, L. Smiri, Y. Laligant, and A. Le Bail, *J. Solid State Sci.* **2,** 285 (2000).
7. L. B. Taher, S. Chabchoub, and L. Smiri-Dogguy, *J. Solid State Sci.* **1,** 15 (1999).
8. D. W. Jones and J. A. S. Smith, *Nature* **195,** 1090 (1962).
9. A. C. Chapman and L. E. Thirlwell, *Spectrochim. Acta* **20,** 937 (1964).
10. E. E. Berry and C. H. Baddiel, *Spectrochim. Acta* **23,** 1781 (1967).

11. E. E. Berry and C. H. Baddiel, *Spectrochim. Acta* **23,** 2089 (1967).
12. K. I. Petrov, B. Soptrajanov, N. Fuson, and J. R. Lawson, *Spectrochim. Acta* **23,** 2637 (1967).
13. K. I. Petrov, B. Soptrajanov, and N. Fuson, *Z. Anorg. allg. Chem.* **358,** 178 (1968).
14. A. C. Chapman, D. A. Long, and D. T. L. Jones, *Spectrochim. Acta* **21,** 633 (1965).
15. W. Yellin and W. A. Celley, *Spectrochim. Acta* **25,** 879 (1969).
16. I. H. Joe, V. S. Jayakumar, and G. Aruldhas, *J. Solid State Chem.* **120,** 343 (1995).
17. K. Viswanathan, V. U. Nayar, G. Aruldhas, and V. Ramakrishnan, *J. Solid State Chem.* **77,** 394 (1988).
18. P. E. Werner, L. Eriksson, and M. Westdhal, *J. Appl. Crystallogr.* **18,** 367 (1985).
19. M. Evain, U-FIT: A cell parameter refinement program, I.M.N., Nantes, France, 1992.
20. L. J. Farrugia, WinGX: An Integrated System of Windows Programs for the Solution, Refinement and Analysis of Single Crystal X-Ray Diffraction Data, University of Glasgow, UK, 1998.
21. N. E. Brese and O'Keeffe, *Acta Crystallogr. B* **47,** 192 (1991).
22. R. D. Shannon, *Acta Crystallogr. A* **32,** 751 (1976).
23. I. D. Brown, *Acta Crystallogr. A* **32,** 24 (1976).
24. E. Kemnitz, C. Werner, and S. I. Trojanov, *Eur. J. Solid State Inorg. Chem.* **33,** 581 (1996).
25. W. G. Fateley, F. R. Dollish, N. T. McDevitt, and F. F. Bentley, "Infrared and Raman Selection Rules for Molecular and Lattice Vibrations: The Correlation Method," Wiley–Interscience, New York, 1972.
26. K. Nakamoto, "Infrared and Raman Spectra of Inorganic and Coordination Compounds," 4th ed., p. 138. Wiley–Interscience, New York, 1986.
27. B. Marchon and A. Novak, *J. Chem. Phys.* **78,** 2105 (1983).
28. K. Vishwanathan, V. U. Nayar, and G. Aruldhas, *Indian J. Pure Appl. Phys.* **24,** 222 (1986).
29. D. Hadzi and S. Bratos, "In the Hydrogen Bond," Vol. 2, p. 565. North- Holland, Amsterdam, (1976).
30. G. L. Hofacker, Y. Marechal, and M. A. Ratner, "In the Hydrogen Bond," Vol. 1, p. 295. North-Holland, Amsterdam, 1976.
31. B. K. Choi, M. N. Lee, and J. J. Kim, *J. Raman Spectrosc.* **20,** 11 (1989).
32. M. Thérèse and P. Ledent, *J. Solid State Chem.* **23,** 147 (1978).
33. M. Bellotto, G. Busca, C. Cristiani, and G. Groppi, *J. Solid State Chem.* **117,** 8 (1995), and references therein.